Enhanced UAV Localization and Outlier Detection Using SVD-Enhanced UWB for Bridge Inspections

Chia-Lun Tsai and Ruey-Beei Wu, *Life Fellow, IEEE*

***Abstract*—This study presents an improved ultrawideband (UWB) positioning algorithm for uncrewed aerial vehicles (UAV) performing bridge inspections. The algorithm uses a two-stage singular value decomposition (SVD) to reduce positioning errors caused by tilted anchor configurations. By evaluating the condition number of the anchor configuration during initial placement, the root-mean-squares error (RMSE) is reduced to one-eighth of the value for the original method at nearly 10° tilt. Optimal anchor placement strategies were further explored, analyzing both noncoplanar and coplanar arrangements. While noncoplanar configurations can enhance accuracy when anchor heights are large, coplanar layouts generally provide greater stability, and square arrangements provide better positioning accuracy. Finally, the SVD-based outlier detection method is also introduced in coplanar configurations. Unlike traditional Dilution of Precision (DoP) methods, where different positioning algorithms produce different DoP values, the proposed method requires only anchor coordinates and measured distances, thereby achieving more accurate outlier detection and robust performance in bridge inspection environments.**

***Index Terms*—Bridge inspection, outlier detection, singular value decomposition (SVD), trilateration, ultrawideband (UWB), uncrewed aerial vehicles (UAV).**

I. Introduction

SINCE Apple introduced ultrawideband (UWB) technology in the iPhone 11 in 2019, UWB has been widely used in commercial applications for high-precision positioning. Market research indicates that the UWB market was worth $1.481 billion in 2021, and is expected to reach $3.638 billion by 2027, which is an annual growth rate of 16.09% [1]. Known for its superior accuracy, low latency, and robust interference resistance [2], UWB is widely applicable in areas such as national security [3], smart home, autonomous driving, and smart logistics [4]. Therefore, this technology is expected to play an essential role in the Internet of Things (IoT).

UWB technology also shows great potential in uncrewed aerial vehicle (UAV) inspections, especially for infrastructure maintenance tasks such as bridge inspections. UAVs are highly maneuverable and flexible, able to enter areas that are difficult for humans to reach and conduct safe and efficient inspections [5]. However, due to obstructions and signal interference from the reinforced concrete often used in bridge construction, precise positioning of UAVs in under-bridge environments is challenging, making traditional GPS-based systems unreliable [6]. Furthermore, the limited lighting under bridges reduces the effectiveness of vision-based positioning methods [7], while the presence of pillars in the bridge structure introduces multipath effects that increase positioning errors [8].

The area under the bridge is characterized by the absence of GPS signals. Many studies turn to vision-based positioning methods, such as simultaneous localization and mapping (SLAM) and visual odometry (VO) [9]. These techniques rely on sensors that are mounted on the UAV, such as RGB or RGB-D cameras, which capture images of the environment and determine the UAV's position through image analysis and feature matching [10]. However, under bridges with weak light and complex structures, the reliability of vision-based positioning methods is significantly poor [11].

With its strong anti-interference ability and high accuracy, UWB technology has become a promising solution for high-precision positioning under bridge. UWB signals are transmitted in the form of pulses, which can effectively reduce multipath effects and achieve stable positioning performance [2]. However, UWB signals are still affected by obstacles under bridge structures, such as pillars, which can result in signal occlusions and lead to ranging errors, thus affecting overall positioning accuracy [12].

Some UWB use strictly coplanar configurations [13], and only few concern with near-coplanar placement of anchors, which will increase condition number and significantly amplify the positioning errors. However, in real-world scenarios such as bridge inspection, near-coplanar placement is often unavoidable due to terrain constraints. Uneven terrain limits the placement of anchors to accessible heights, usually near human working levels. In contrast, bridges are usually built in such a way that the deck is horizontal. Therefore, it happens that the bridge deck is not parallel to the terrain ground. This misalignment can impact positioning accuracy, leading to poor performance of Taylor-series algorithm and the original two-stage methods.

This study proposes a two-stage positioning method based on singular value decomposition (SVD) to reduce positioning errors in near-coplanar configurations by checking the condition number during the initial anchor placement phase. Additionally, this study also analyzes root-mean-squares error (RMSE) trends for noncoplanar configurations to determine

Received 20 March 2025; revised 2 April 2025 and 19 April 2025; accepted 15 May 2025. Date of publication 19 May 2025; date of current version 8 August 2025. This work was supported in part by the Ministry of Science and Technology, Taiwan, under Grant MOST 110-2221-E-002-172, and in part by PSJ Inc. *(Corresponding author: Chia-Lun Tsai.)*

The authors are with the Department of Electrical Engineering and the Graduate Institute of Communication Engineering, National Taiwan University, Taipei 106, Taiwan (e-mail: galant4456@gmail.com; rbwu@ntu.edu.tw).

Digital Object Identifier 10.1109/JIOT.2025.3571543

the most effective anchor deployment strategies across different terrains.

To increase system reliability, an SVD-based outlier detection method is designed to identify and correct positioning errors caused by occlusion effects, particularly useful in challenging environments such as under bridges. In real-time positioning applications in the industry, the Dilution of Precision (DoP) metric is often used to assess the accuracy of positioning data [14]. However, different positioning algorithms may produce different coordinates, resulting in different DoP values. This lack of a unified standard makes it challenging to consistently evaluate positioning accuracy using different methods [15]. Therefore, building on SVD-based positioning method, this study proposes an outlier detection method to effectively identify and correct errors, thereby enhancing the robustness of the positioning system in complex environments.

This study makes the following contributions.

1) An SVD-based algorithm is proposed that outperforms the original two-stage method for tilted anchor configurations. It achieves 8 times better RMSE at 10° tilt.
2) While noncoplanar anchor configurations can improve RMSE at certain heights, it is shown that coplanar configurations, especially square layouts, give the best overall performance.
3) For positioning using coplanar anchors, an SVD-based outlier detection method is proposed that identifies measurement errors using only the measured distances and true anchor coordinates.

The remainder of this study is organized as follows. Section II describes the real-world challenges of positioning in under-bridge environments, followed by calibration methods and an description of the SVD-based positioning algorithm. Section III presents simulations and a tilted plane experiment to verify the accuracy of the algorithm in near-coplanar conditions. Section IV provides an analysis of noncoplanar configurations, examining RMSE trends to determine optimal anchor deployment strategies. Section V introduces the SVD-based outlier detection method, including real-world experiments simulating an under-bridge environment to evaluate the robustness of the method. Finally, Section VI summarizes the study results.

II. Theory

A. Statement of Problem

The UAVs are equipped with sensors and camera to conduct inspection under bridges. UWB technology was utilized for UAV positioning, and experiments were performed on two bridges: 1) the Pinghu No. 7 Bridge and 2) the Wanshou Bridge, located in the Taipei suburbs [16]. In this study, the positioning challenges posed by these two specific bridge structures are addressed. The Pinghu No. 7 Bridge has a total length of 85 m. The terrain under the bridge is on tilted slope, and the placement of anchors and the positioning accuracy is complicated. In addition, the larger Wanshou Bridge is 166 m long and has multiple pillars, which may require noncoplanar anchor placement, so UAV positioning is more complex.

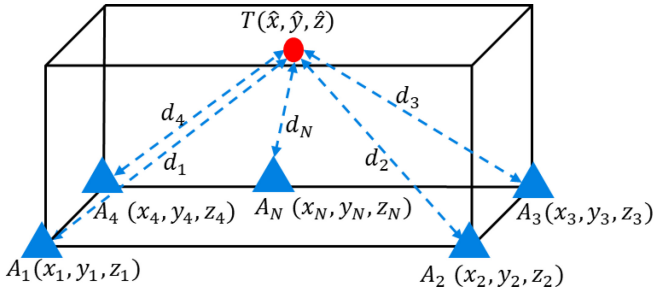

Fig. 1. Schematic of 3-D positioning using multiple anchors.

Traditionally, positioning techniques such as trilateration and least-squares estimation [17] are often used to solve positioning problems. However, these methods frequently produce inaccurate results under near-coplanar anchor configurations. This is because the near-coplanar setup of anchors has a narrow span in a certain dimension, which results in a significant increase in the condition number of the positioning matrix, as shown in the subsequent derivation, thereby reducing the stability of the matrix solution. In such cases, the positioning results become sensitive to the smallest singular values of the matrix, which means that even a small perturbation may lead to a large positioning error. Although iterative methods such as the Taylor-series algorithm can address this issue [18], but multiple iterations are required so the computation time increases and they are unsuitable for real-time positioning applications.

A two-stage method was proposed to obtain the accurate altitude of the device under test (DUT) when the anchors are on the ground and at the same altitude [19]. The horizontal coordinates are solved by least-squares solution, while the altitude is obtained separately by solving the zeros of a cubic polynomial equation. However, if the anchors are located nearly coplanar on sloping terrain, the unequal altitudes of the anchors will greatly contaminate the accuracy of the horizontal coordinates, resulting in inaccurate DUT positioning. To overcome these limitations, this study proposes an enhanced two-stage method based on SVD to improve accuracy in complex under-bridge environments. The method measures the condition number of the positioning matrix to significantly reduces positioning errors and improves altitude precision in near-coplanar scenarios, providing a more robust solution compared to the original two-stage method.

B. SVD-Based Two-Stage Trilateration

In a positioning scenario for $N = 4$ or more anchors, let the coordinates of the DUT at point $T(\hat{x}, \hat{y}, \hat{z})$ and the coordinates of the anchors be $A_i(x_i, y_i, z_i)$ for $i = 1 \sim N$ as shown in Fig. 1. Given that the distance between the DUT and the ith anchor is d_i, it can be expressed as

$$\sqrt{(\hat{x}-x_i)^2+(\hat{y}-y_i)^2+(\hat{z}-z_i)^2}=d_i. \tag{1}$$

For the triangle that is formed by the reference anchor A_N, a given anchor A_i and the DUT, as shown in Fig. 2, let the

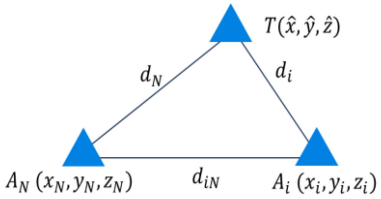

Fig. 2. Triangle configuration of A_N, A_i, and DUT.

distance between the A_N and A_i be d_{iN}. The cosine law to express the dot product of vector $\overrightarrow{A_NA_i}$ and vector $\overrightarrow{A_NT}$ as

$$\overrightarrow{A_NA_i}\cdot\overrightarrow{A_NT} = \frac{1}{2}\left({d_N}^2 + {d_{iN}}^2 - {d_i}^2\right). \tag{2}$$

For a total of N anchors, they can be organized into a matrix form

$$\boldsymbol{A}X = B \tag{3}$$

where

$$\boldsymbol{A} = \begin{bmatrix} x_1 - x_N & y_1 - y_N & z_1 - z_N \\ x_2 - x_N & y_2 - y_N & z_2 - z_N \\ \vdots & \vdots & \vdots \\ x_{N-1} - x_N & y_{N-1} - y_N & z_{N-1} - z_N \end{bmatrix}_{(N-1)\times 3}$$

$$X = \begin{bmatrix} \hat{x} - x_N \\ \hat{y} - y_N \\ \hat{z} - z_N \end{bmatrix}_{3\times 1}; B = \frac{1}{2}\begin{bmatrix} {d_N}^2 + {d_{1N}}^2 - {d_1}^2 \\ {d_N}^2 + {d_{2N}}^2 - {d_2}^2 \\ \vdots \\ {d_N}^2 + {d_{N-1,N}}^2 - {d_{N-1}}^2 \end{bmatrix}_{(N-1)\times 1.}$$

This study applies SVD method to solve (3). Starting with the SVD decomposition on the matrix $\boldsymbol{A}$, rewrite $\boldsymbol{A}X = B$ as $\boldsymbol{U}\boldsymbol{\Sigma}\boldsymbol{V}^TX = B$. Here, $\boldsymbol{U}$ and $\boldsymbol{V}$ are unitary matrices and $\boldsymbol{\Sigma}$ is a diagonal matrix consisting of singular values of $\boldsymbol{A}$, *i.e.,* λ_i $(i = 1,\ 2,\ 3)$. Multiplying both sides of (3) by $\boldsymbol{U}^T$ gives

$$\boldsymbol{\Sigma}\left(\boldsymbol{V}^TX\right) = \boldsymbol{U}^TB. \tag{4}$$

Accordingly, X has been transformed into the V domain. Define the solution of X in the V domain as $\boldsymbol{V}^TX = X'$, with coordinates $(x',\ y',\ z')$.

A typical way to find the SVD of a matrix $\boldsymbol{A}$ is to compute the matrix product $\mathbf{A}^T\mathbf{A}$, whose eigenmatrix is $\boldsymbol{V}$ and eigenvalues p's correspond to squares of the singular values of the matrix $\mathbf{A}$, i.e., $p_i = \lambda_i^2$. For example, consider four anchors (N=4) with coordinates $(x_i,\ y_i,\ z_i)$ $(i = 1, .., N)$ at $(a,\ 0,\ 0)$, $(0, b, 0)$, $(a,\ b,\ c)$ and $(0,\ 0,\ 0)$, respectively. Assume that $a,\ b,\ c$ are all positive real numbers and $c \ll b \leq$ a. It is not difficult to derive the cubic equation that p satisfies. It can be solved analytically using the Cardano expression, but a simpler form can be derived for small c. The roots are $p_{1,2} \cong (a^2 + b^2) \pm \sqrt{a^4 - a^2b^2 + b^4}$ and $p_3 \cong (c^2/3)$. The singular values of matrix $\boldsymbol{A}$ are $\lambda_i = \sqrt{p_i}$ and the condition number $\kappa(\boldsymbol{A}) = (\lambda_1/\lambda_3)$. It clearly depicts how a small c deteriorates the condition number.

It is known that $\kappa(\boldsymbol{A})$ is defined more precisely to be the maximum ratio of the relative error in X to the relative error in B in (3). Let e be the error in B, then the error in the solution $\boldsymbol{A}^{-1}B$ is $\boldsymbol{A}^{-1}$e. The ratio of the relative error in solution X to the relative error in B is

$$M = \frac{\frac{\left\|A^{-1}e\right\|}{\|X\|}}{\frac{\|e\|}{\|B\|}} = \frac{\left\|A^{-1}e\right\|}{\|e\|}\cdot\frac{\|\mathrm{AX}\|}{\|X\|}. \tag{5}$$

Here, the norm is the matrix norm induced by the (vector) Euclidean norm (also known as the L^2 norm and typically denoted as), and $\boldsymbol{A}X$ replaces B. The maximum value (for nonzero B and e) can be expressed as the product of the two operator norms as follows:

$$\max_{X,B\neq 0} M \leq \left\{\max_{e\neq 0}\frac{\left\|A^{-1}e\right\|}{\|e\|}\right\}\cdot\left\{\max_{X\neq 0}\frac{\|X\|}{\|\mathrm{AX}\|}\right\} \leq \frac{1}{\lambda_3}\cdot\lambda_1 \tag{6}$$

which is equal to $\kappa(\boldsymbol{A})$.

For the originally proposed solution [19], the least-squares method is used to solve (3). In near-coplanar anchor configurations, the condition number of $\boldsymbol{A}$ matrix becomes excessively high. Even a small error in distance measurements can lead to inaccurate positioning in the 2-D calculation, which in turn results in an even larger error in the second stage of solving for $\hat{z}$.

The present method performs SVD on matrix $\boldsymbol{A}$ and solves for X' in the new coordinate system. Since the column vectors in $\boldsymbol{V}$ are orthogonal, so there is an orthogonal basis in the V domain, thus simplifying the structure of the $\boldsymbol{A}$ matrix. This allows us to solve efficiently within this transformed coordinate system, as matrix inversion for (3) is no longer required.

The solution for X' in (4) is easy because Σ is a diagonal matrix of singular values. If the condition number exceeds a certain threshold, the terms associated with the smallest singular value λ_3 are removed to minimize their effect on positioning accuracy. By reducing the influence of the smallest singular values, a more accurate solution for coordinates $(x',\ y')$ is derived. The error multiplication factor M in (5) can be significantly reduced from λ_1/λ_3 to λ_1/λ_2, and the overall positioning accuracy is increased. This completes the stage-one solution. The third unknown can be determined through optimization in the second stage. In the coplanar case, $\lambda_3 = 0$, and simply removing λ_3 still allows the method to function properly.

This calculation is performed in the V domain so the anchor coordinates are multiplied by converting them to the V domain. Let the transformed anchor matrix is $\boldsymbol{A}'$. The reference point coordinates are added back to give the coordinates of N anchors in the V domain, denoted as (x_i', y_i', z_i') for $i = 1 \sim N$.

The second-stage solution involves a cost function proposed in [19], which is defined as follows:

$$\sum_{i=1}^{i=N}\left[\left(d_i^2 - (x' - x_i')^2 + \left(y' - y_i'\right)^2 + \left(z' - z_i'\right)^2\right)^2\right]. \tag{7}$$

To solve for z', the partial derivative of (7) with respect to z' is calculated and the solution is simplified to a cubic equation for z', which is solved using Cardano's formula.

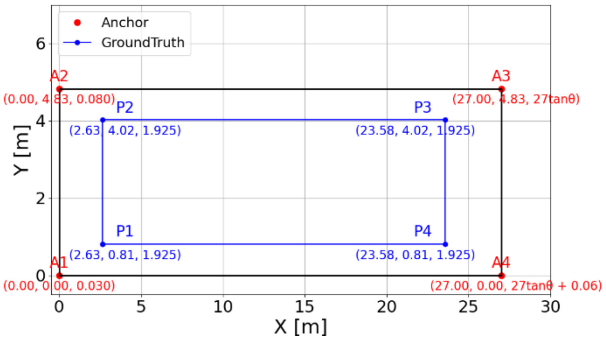

Fig. 3. Anchor positions and walking path on tilted plane.

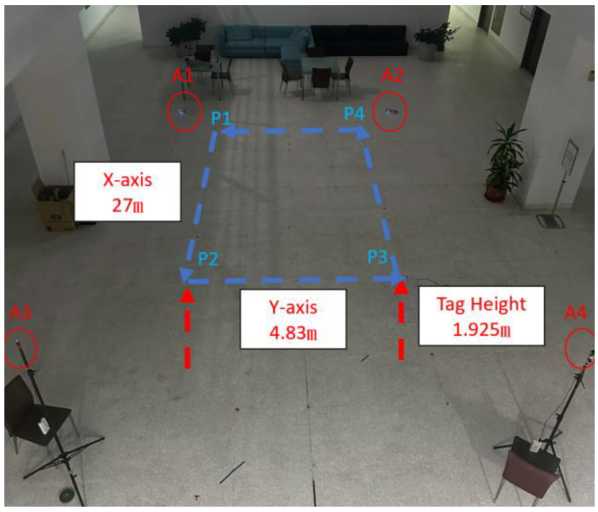

Fig. 4. Experimental setup for tilted plane.

After (x', y', z') is calculated in the V domain and multiplied by the $\boldsymbol{V}$ matrix to convert to Euclidean space, so the DUT position is defined in the original coordinate system.

Thus, the overall complexity remains $O(1)$, as all operations involve fixed 3×3 matrices. Different from the iterative Taylor-series algorithm [19], our method ensures faster convergence with minimal computational cost.

III. Experimental Validation For Tilted Plane

The scenario for Pinghu No. 7 Bridge is simulated. The bridge has a total length of 85 m and a maximum width of 12 m, with an open space below that is inclined at 10°. The simulation varies this tilt angle from 0° to 10° to examine the effects of different tilted planes on positioning accuracy.

A. Simulation for Tilted Plane

Consider an area 27 m long and 4.83 m wide, where four UWB anchors $A1$, $A2$, $A3$, and $A4$ are located near the vertices, as shown in Fig. 3. $A1$ is placed at a height of 0.03 m, $A2$ at 0.08 m, and the placement height of the remaining two anchors $A3$ and $A4$ changes with the tilt angle according to the slope. Specifically, $A3$ is set at a height of $27 \tan\theta$ m, and $A4$ at $27 \tan\theta + 0.06$ m. For this setting, θ varies from 0° to 10° to simulate different near-tilted plane.

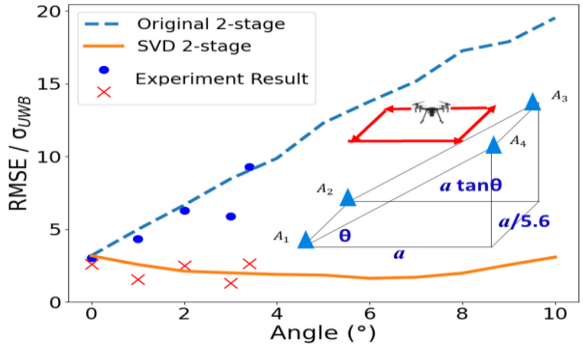

Fig. 5. Comparison of experimental and simulation results for positioning accuracy.

At the beginning of the experiment, a participant walked along a rectangular path with a fixed height, starting from point $P1$ at coordinates (2.63, 0.81, 1.925), passing counter-clockwise through points $P2$, $P3$, and $P4$, and finally returning to $P1$, as shown in Fig. 4.

For simulation, the DUT is located at a fixed height of 1.925 m within a rectangular path. The sampling points are evenly distributed, with 100 points along the length and 100 along the width, to give a route of 400 points. The height of these 400 points is fixed at 1.925 m. Gaussian noise with a mean of 0.2 m and a standard deviation of 0.05 m is added to the distance measurements to simulate measurement errors.

B. Experiment for Tilted Plane

The tilted plane experiment was conducted on the fifth floor of the Ming Da Hall at National Taiwan University. This experiment used a Decawave DWM1000 UWB module that was provided by GIPS Inc., which can be connected to the RPi 4B through the UWB communication protocol to read distance data. The Android app DW Tag Monitor, which is also from GIPS Inc., was used to configure the UWB module to operate at a center frequency of 3.5 GHz (CH2) with a bandwidth of 500 MHz.

The third and fourth anchors were raised using tripods. At the anchor positions, the $A1$ anchor was used as the origin point and a tape measure was used to determine the coordinates of the other three anchors. A laser pointer was then used to measure the heights of all four anchors to ensure accurate placement. Since the maximum height of the tripods is 1.61 m, the tilt angle in experiment was limited to 3.4°. Fig. 4 shows the experimental setup, where the locations of anchors and the participant paths are the same as in the simulation.

For this setting, 3-D positioning error is defined as the RMSE between the positioning result and the ground truth. Fig. 5 compares the RMSE values for the original two-stage method and the SVD-enhanced two-stage method as the tilt angle changes in simulation and experiment. The blue dashed line represents the RMSE of the original two-stage method in simulation, and the orange solid line represents the RMSE of the SVD-enhanced two-stage method in simulation. The crosses and dots are the experimental data.

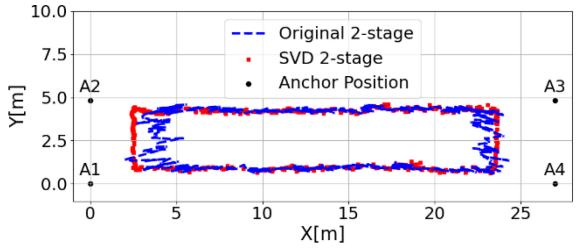

Fig. 6. Comparison of original and SVD two-stage methods for 2-D positioning at tilt angle $\theta = 3.4^{o^\circ}$.

The figure shows that the RMSE for the original method rises significantly as the tilt angle increases, especially over 2°, reaching a peak at 10°, where the RMSE is approximately 8 times higher than at 0°. In comparison, the SVD two-stage method maintains stable and lower RMSE across different angles, keeping it below $3\sigma_{\text{UWB}}$, where σ_{UWB} represents the UWB measurement error. This threshold of $3\sigma_{\text{UWB}}$ signifies high accuracy, as it limits the positioning error to three times the expected measurement error, so this method is robust for tilted planes.

The figure shows that the RMSE for the original method rises significantly as the tilt angle increases, especially over 2°, reaching a peak at 10°, where the RMSE is approximately 8 times higher than at 0°. In comparison, the SVD two-stage method maintains stable and lower RMSE across different angles, keeping it below $3\sigma_{\text{UWB}}$, where σ_{UWB} represents the UWB measurement error. This threshold of $3\sigma_{\text{UWB}}$ signifies high accuracy, as it limits the positioning error to three times the expected measurement error, so this method is robust for tilted planes.

The effect of the smallest singular value on the positioning results is also determined. At a tilt angle of 3.4°, the condition number is 606 and the smallest singular value $\lambda_3 = 0.0634$. This small value represents a high sensitivity to measurement errors, which can significantly affect the 2-D positioning results. A comparison for the 2-D positioning results of the two-stage methods under these conditions is shown in Fig. 6.

The positioning errors for the three axes are calculated separately. The results are shown in Table I, where the proposed method is also compared with the Taylor-series algorithm. It shows a significant speed-up in computation time. Here, the results of the original two-stage method are used as the initial guess for the Taylor-series algorithm. It is found that convergence is achieved in 7.5 iterations on average, while the CPU time is approximately twice that of the SVD-based method.

For y-axis positioning, the difference between the SVD two-stage method and the original two-stage method is small. These results show that in actual positioning experiments, using SVD can significantly improve x-y positioning accuracy and reduce error amplification caused by a high condition number.

IV. Discussion For Noncoplanar Scenarios

As discussed in Section II, noncoplanar placement is common for under-bridge positioning scenarios. Current research, such as one 2024 study [20], focuses on a specific scenario where the DUT is located at a fixed height and has different aspect ratios. However, these studies ignore more complex possibilities, such as different anchor heights, which can significantly affect positioning accuracy and efficiency. Theoretically, as the anchor height increases, additional information along the z-axis should be gained, which is expected to reduce RMSE.

In Section II, the positioning algorithm is used to transform the coordinates into the V domain, allowing any coordinate configuration in Euclidean space to be mapped to this new coordinate system, in which the coordinates of the three noncollinear anchors must form a plane, and the fourth anchor has a specific height difference relative to this plane. This configuration is used to determine how this height difference affects RMSE.

TABLE I
Comparison of Mean Error for X and Y Axes Using the Original and SVD Two-Stage Methods and the Taylor-Series Algorithm

Method	Mean Error(m)		Per-point CPU Time (ms)
	X-axis	Y-axis	
Two-stage (original)	1.0191	0.2003	0.083
Two-stage (SVD)	0.0485	0.1894	0.078
Taylor-series algorithm	0.0820	0.1521	0.16

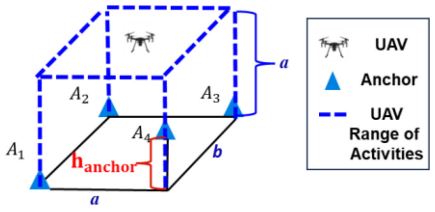

Fig. 7. Simulation setup for noncoplanar anchor configuration.

A. Simulation for Noncoplanar Scenario

This scenario uses an aspect ratio of 1 to give a square configuration with side length a. The fourth anchor is located at different heights, and the anchor arrangement is shown in Fig. 7. As shown in Fig. 7, the configuration has length of a and width of b, forming a rectangular arrangement. In this simulation, a equals b. The DUT sampling points are evenly distributed within this square area, and the x and y coordinates are sampled at intervals of $(a/30)$, providing a total of 900 points at a fixed height h_{tag}. To simulate measurement errors, Gaussian noise with mean of 0 and standard deviation of $(a/40)$ is added to the calculated distances that is derived using experimental measurements.

For the simulation, the detailed height-related configurations are shown in Fig. 7. The anchor height h_{Anchor} increases from 0 to a in steps of $(a/50)$, and the DUT height h_{tag} ranges from 0 to a in steps of $(a/50)$.

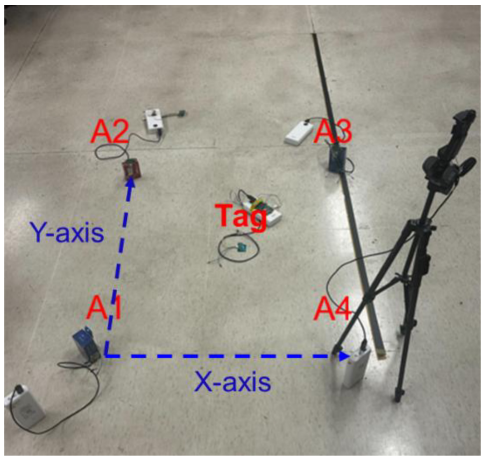

Fig. 8. Experimental setup for noncoplanar RMSE verification.

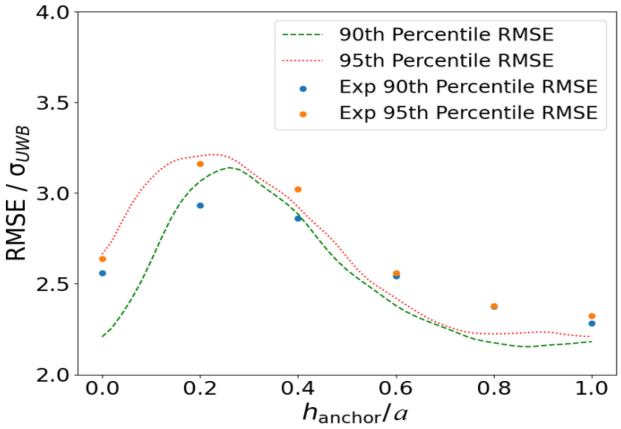

Fig. 9. Comparison of experimental and simulation curves.

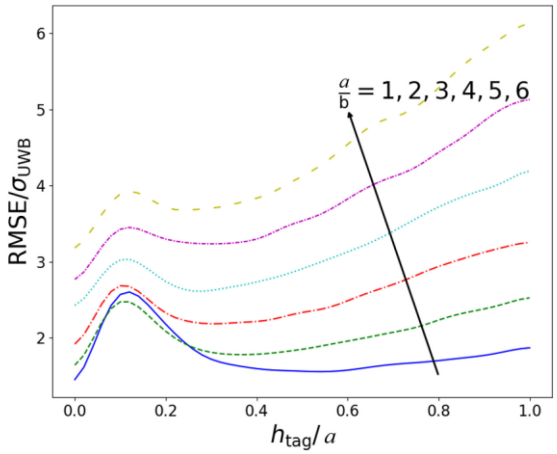

Fig. 10. RMSE with different aspect ratios.

B. Experiment for Noncoplanar Scenario

In Classroom 402 on the fourth floor of the Ming Da Hall of National Taiwan University, a noncoplanar RMSE characteristic curve verification experiment was conducted. Four anchors were placed on the ground to form a square with sides of one meter. The DUT was initially placed at a height of 0 m and this height was gradually increased in 0.1 m steps to 0.4 m. Additionally, the anchor heights were adjusted using tripods, starting at 0 m and increasing to 1 m in 0.2 m intervals. Fig. 8 shows the layout for the experiment.

At each specified height for the tag, the system was calibrated and 100 measurements recorded the RMSE and σ_{UWB}, where σ_{UWB} is the standard deviation of the UWB measurement error. The ratio of RMSE to σ_{UWB} was calculated for the experimental data and the result was compared with that for the simulation RMSE characteristic curve to verify consistency. To better observe the trends, Gaussian smoothing with $\sigma = 1$ was applied, and the relationship between the 90th and 95th percentiles of (RMSE/σ_{UWB}) were then compared for different h_{Anchor} values and the results are shown in Fig. 9.

The figure shows that the RMSE reaches a maximum value between 0.1a and 0.3*a,* but deceases significantly as the anchor height increases to a certain level. This shows that increasing the anchor height to more than 0.6a can significantly improve positioning accuracy, making it an effective strategy for reducing RMSE in noncoplanar configurations.

However, due to practical limitations for the area under the Wanshou Bridge, as mentioned in Section II, the anchor length is 40 m but the bridge height is only 5 m. Fig. 9 shows that the RMSE remains higher in noncoplanar configurations at this limited height. Although an anchor height of 0.6a (approximately 24 m) would theoretically improve positioning accuracy, achieving such a height is not feasible within the structural constraints of most bridge inspection scenarios. Therefore, a coplanar configuration is not only more realistic, but also proves to be the best setting for consistent and reliable positioning in real-world applications.

After confirming the advantages of coplanar configuration, as shown in Fig. 7, the parameters for simulation setup A (where length is a and width is b) are used to determine the effect of tag height and aspect ratios (ranging from 1 to 6) on positioning accuracy with Gaussian smoothing with $\sigma = 2$. As shown in Fig. 10, the RMSE increases with aspect ratio and the square configurations yield the lowest positioning error, with a RMSE of less than $3\sigma_{\text{UWB}}$.

In summary, a noncoplanar setup gives a smaller RMSE value at sufficiently large heights, but the coplanar configurations, especially square layouts, provide the best overall positioning accuracy for bridge inspection using UWB ranging technology. Since the condition number is not excessively large in the discussed scenarios, the performance trend remains similar to the original two-stage method while maintaining stability across different configurations.

V. SVD-Based Outlier Detection

Section IV shows that placing anchors in a coplanar square is the most practical configuration, but under bridges, anchors are often obstructed by beams and pillars. Therefore, this study proposes an outlier detection method that is specific to coplanar anchor settings.

A. Method

Using SVD decomposition, $AX = B$ is rewritten as (4) where

$$\boldsymbol{U}^T = \begin{bmatrix} u_{11} & u_{21} & \dots & u_{N-1,1} \\ u_{12} & u_{22} & \dots & u_{N-1,2} \\ \vdots & \vdots & \dots & \vdots \\ u_{1,N-1} & u_{2,N-1} & \dots & u_{N-1,N-1} \end{bmatrix}_{N-1\times N-1}$$

$$B = \frac{1}{2}\begin{bmatrix} {d_N}^2 + {d_{1N}}^2 - {d_1}^2 \\ {d_N}^2 + {d_{2N}}^2 - {d_2}^2 \\ \vdots \\ {d_N}^2 + {d_{N-1,N}}^2 - {d_{N-1}}^2 \end{bmatrix}_{(N-1)\times 1}.$$

For four coplanar anchors, the corresponding $\boldsymbol{\Sigma}$ matrix has nonzero λ_1 and λ_2, while λ_3, corresponding to the z'-direction, must be zero.

Based on this property, the last element of $\boldsymbol{U}^T B$ which generally takes the following form:

$$P \equiv C + \sum_{i=1}^{N} a_i {d_i}^2 \tag{8}$$

and must be zero, in which

$$C = \frac{1}{2}\left(u_{1,N-1}{d_{1N}}^2 + \ldots + u_{N-1,N-1}{d_{N-1,N}}^2\right)$$

and a_i represents the terms derived from the coefficients in the last row of Matrix $\boldsymbol{U}^T$, each of which is scaled by $(1/2)$. d_i is the true distance between the ith anchor and tag.

Consider that there is measurement error for real-world conditions. $\hat{d}_i$ is the measured distance between the ith anchor and tag, and the measurement error obeys a normal distribution of mean d_i and standard deviation σ_{UWB}. Then, expected value and variance of $\hat{P}$ are

$$E\left[\hat{P}\right] = \sum_{i=1}^{N} a_i \sigma_{\text{UWB}}^2 \tag{9}$$

$$\text{Var}\left[\hat{P}\right] = \sum_{i=1}^{N} {a_i}^2 Var\left(\hat{d}_i^2\right). \tag{10}$$

The random variable $X_i = d_i + N_i$. In terms of the properties of a normal distribution, X_i also obeys normal distribution, which is given by $X_i \sim N(0, \sigma_{\text{UWB}}^2)$. The variance of this random variable X_i^2 is calculated as

$$\text{Var}\left(X_i^2\right) = E\left[X_i^4\right] - \left(E\left[X_i^2\right]\right)^2. \tag{11}$$

Using the fourth moment formula gives

$$\text{Var}\left(X_i^2\right) = 4{d_i}^2\sigma_{\text{UWB}}^2 + 2\sigma_{\text{UWB}}^4 \tag{12}$$

by expanding and simplifying the terms. Therefore

$$\text{Var}\left(\hat{P}\right) = 4\sigma_{\text{UWB}}^2 \sum_{i=1}^{N} {a_i}^2 \left[{d_i}^2 + \frac{1}{2}\sigma_{\text{UWB}}^2\right]. \tag{13}$$

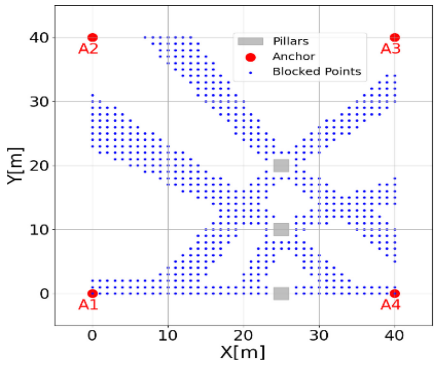

Fig. 11. Distribution of occlusion by pillars.

Given that the square of the true distance is much greater than the variance for the standard deviation, so the standard deviation of P is approximated as

$$\sigma_P \cong 2\sigma_{\text{UWB}} \sqrt{\sum_{i=1}^{N} {a_i}^2 {d_i}^2}. \tag{14}$$

This formula does not require positioning results; it only requires anchor coordinates and measured distances.

B. Simulation for Pillar Obstructions Scenarios

The real situation under the Wanshou Bridge is simulated to determine the effect of beam and pillar obstructions on UAV inspections in the bridge environment. To better represent real-world conditions, the pillar layout is modelled under the Wanshou Bridge to simulate the pillar arrangement and UWB signal coverage. Each pillar measures 2 m × 2 m × 5 m, and UWB testing shows that there is an effective coverage area of 40 m × 40 m.

Before simulating outliers, the probability of obstruction in this area is calculated. Sample points are placed every 0.5 m in a space of 40 m × 40 m × 5 m to measure the obstruction of UAV by the pillars. For each sample point, the lines connecting it to the four anchors are checked and if any line is blocked by a pillar, the point is denoted as obstructed. As shown in Fig. 11, the probability of obstruction is 0.39.

To ensure UAV safety during flight, the practical operation guideline of GIPS Inc. were observed by setting the flight height at about 3 m to avoid collision with the bridge structure above. This adjustment defines the UAV's operational space as 40 m × 40 m × 3 m. 80 points were sampled along each side of the anchor's length and width and 6 points along the height, to give a total of 38 400 measurement points.

For the simulation, each measurement point has a 40% chance of obstruction. First, a pillar of 0.97 × 0.85 m^2 was measured, showing an additional occlusion range of 0.1–0.6 m. Given the 2 × 2 m^2 pillar in our setup, it is scaled up to 0.2–1.2 m. This effect is incorporated into the outlier detection model using a uniform distribution to simulate signal interference. To analyze the effects of different occlusion distances, 5000 uniformly distributed occlusion distances were generated between 0.2 and 1.2 m and simulated individually. The remaining measurements were using Gaussian noise with

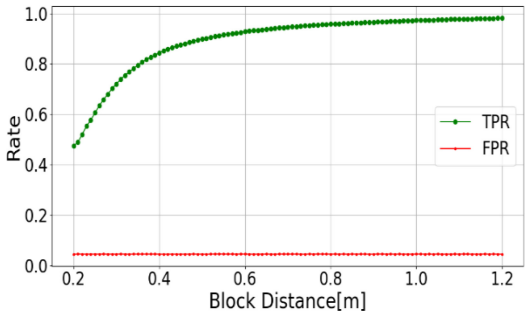

Fig. 12. TPR and FPR versus obstruction distance.

TABLE II
CONFUSION MATRIX AND EVALUATION METRICS FOR OUTLIER DETECTION

Actual	Predict		
	Positive	Negative	Evaluation
Positive	TP : 0.3595	FN : 0.0405	TPR: 0.8988
Negative	FP : 0.0269	TN : 0.5731	FPR: 0.0448
Evaluation	Precision: 0.9305		Accuracy: 0.9327

a mean of 0 and a standard deviation of 0.05 m, to represent standard measurement variation.

The threshold that identifies outliers under these conditions is then determined. Since the block distances are relatively small compared to the true distances, even when incorporating measured distances with errors, the calculated standard deviation remains closely identical to the value calculated by the true distances. Therefore, when using this formula, the measured distances are directly substituted to calculate σ_P.

The normal value of $U^T B$ obeys chi-squared distribution with a degree of freedom of 4, and the distribution closely approximates a Gaussian distribution. For outlier detection, twice σ_P is used is used as the criterion based on the 66-95-99.7 rule, covering approximately 95% of normal values to ensure most normal points are correctly classified. Once the DUT obtains the measured distances, it calculates the last value of $U^T B$. If this value exceeds the threshold, it is classified as an outlier.

A confusion matrix [21] is used to verify the simulation results and analyze variations for different obstruction distances to evaluate the reliability of the detection model. The algorithm's performance is determined using key metrics that are commonly used for outlier detection. These four metrics are: 1) true positive rate (TPR); 2) false positive rate (FPR); 3) precision; and 4) accuracy. They are, respectively, calculated as TPR $=$ (TP/TP + FN), FPR $=$ (FP/FP + TN), *Precision* $=$ (TP/$TP + FP$), and *Accuracy* $=$ ($TN + TP/TP + FP + FN + TN$), respectively.

Table II lists the results for these evaluation metrics. The TPR is 0.8988, so the model accurately detects 89.88% of anomalies. Anomaly detection is highly satisfactory. The FPR is 0.0448, so the false alarm rate is only 4.48%. This shows that the model occasionally misclassifies normal points as anomalies, but the overall false alarm rate is low. The *Precision* value is 0.93, so the model accurately predicts an anomaly 93% of the time, which is highly accurate anomaly detection. The overall *Accuracy* is 0.9327, so the model achieves an overall accuracy of 93.27% for all measurement points and features stable performance.

In addition, to understand how model performance changes as the obstruction distance increases, the variations in TPR and FPR are calculated under different obstruction distances and the results are plotted in Fig. 12. After sorting the obstruction distance data, it is divided into intervals of 0.01 m, and the TPR and FPR are calculated for each interval. As the obstruction distance increases, the TPR increases steadily and exceeds 0.95 at around 0.8 m, indicating that the outlier detection accuracy is improved under greater obstruction distances. The FPR remains around 0.045 and shows the strong stability in identifying normal values.

It is worth noting that in a 40 m $\times$ 40 m space, with an increase of 0.22 m of random error per point, the TPR of the model reaches 0.5, indicating that even under conditions where the random error significantly smaller than the spacing between anchors, there is a 50% likelihood of correctly identifying outliers. This shows that the model is robust to obstructions and can reliably detect outliers even with minor errors, ensuring more dependable predictions.

VI. CONCLUSION AND DISCUSSION

This study determines the effect of anchor configurations on tilted planes and shows that if the condition number for the positioning matrix is too large, the positioning error for the original two-stage method increases significantly. Specifically, when the tilt angle exceeds 2°, the SVD algorithm effectively reduces the RMSE to one-third of that for the original algorithm. At a tilt angle of 10°, the SVD algorithm reduces the RMSE to one-eighth of the value for original method. This is a significant increase in accuracy.

Noncoplanar anchor configurations are studied and the statistical distribution of RMSE for different settings is determined. The results show that for a specific height configuration, a noncoplanar arrangement produces a lower RMSE than a coplanar configuration. However, for practical applications, coplanar configurations provide more stable performance, and square layouts are the most efficient anchor arrangement. Section IV details how to adjust the anchor height for a specific bridge structure and conclude that a coplanar square layout is best suited for the bridge environments for this study. Basically, the cases where the anchors are placed in a rectangular configuration has been thoroughly studied. In the future, it is still needed to investigate the impact of different four-anchor configurations on positioning accuracy.

The second application pertains to the specific challenges of coplanar anchor configurations that are more commonly used in practice. An outlier detection algorithm is used to detect measurement errors due to obstructions in this setting. This detection system performed well in the bridge environment, achieving a TPR of 89.88% and an overall accuracy of 93.27%. This shows that most of the anomalous measurement results

due to obstacles are identified, so positioning and stability are accurate.

For future applications, this enhanced UWB positioning algorithm with UAV technology can significantly improve the efficiency of bridge and infrastructure inspections. Precise positioning and reliable outlier detection algorithms allow the system to maintain consistent performance across diverse environmental conditions, including those that include obstructions that are typical under bridge. Although the present method does not allow flexible adjustment of anchor placement, the proposed outlier detection can effectively identify positioning errors and guide manual adjustments to enhance accuracy and reliability. This technology not only minimizes measurement errors due to anchor configurations, but also increases the accuracy of outlier detection and reliable positioning results.

REFERENCES

[1] J. A. Dhapte (Market Research Future, Pune, India). *Ultra-wideband (UWB) Market Research Report—Global Forecast Till 2027*. Accessed: Feb. 10, 2024. [Online] Available: https://www.marketresearchfuture.com/reports/ultra-wideband-market-2367

[2] R. S. Kshetrimayum, "An introduction to UWB communication systems," *IEEE Potentials*, vol. 28, no. 2, pp. 9–13, Mar./Apr. 2009.

[3] S. Colson and H. Hoff, "Ultra-wideband technology for defense applications," in *Proc. IEEE Int. Conf. Ultra-Wideband*, Zurich, Switzerland, 2005, pp. 615–620

[4] (NXP Inc., Eindhoven, The Netherlands). *Ultra-Wideband Press Kit*. Accessed: Feb. 10, 2024. [Online]Available: https://www.nxp.com/company/about-nxp/newsroom/media-library/ultra-wideband-press-kit:NXP-UWB-TECHNOLOGY-PK

[5] S. Feroz and S. Abu Dabous, "UAV-based remote sensing applications for bridge condition assessment," *Remote Sens.*, vol. 13, no. 1809, 2021.

[6] R. A. Dalke, C. L. Holloway, P. McKenna, M. Johansson, and A. S. Ali, "Effects of reinforced concrete structures on RF communications," *IEEE Trans. Electromagn. Compat.*, vol. 42, no. 4, pp. 486–496, Nov. 2000

[7] Z. Jiang, J. Tan, D. Huang, and Y. Meng, "Robust visual positioning of the UAV for the regional operation," in *Proc. CAA Symp. Fault Detection, Supervis. Saf. Tech. Processes (SAFEPROCESS)*, Yibin, China, 2023, pp. 1–5.

[8] N. Iya, A. Muqaibel, U. Johar, and M. A. Landolsi, "Ultra-wideband characterization of obstructed propagation," in *Proc. 7th Int. Wireless Comm. Mobile Computing Conf.*, Istanbul, Turkey, 2011, pp. 624–629

[9] H. D. K. Motlagh, F. Lotfi, H. D. Taghirad, and S. B. Germi, "Position estimation for drones based on visual SLAM and IMU in GPS-denied environment," in *Proc. 7th Int. Conf. Robot. Mechatron. (ICRoM)*, Tehran, Iran, 2019, pp. 120–124.

[10] W. Aguilar, G. Rodríguez, L. Álvarez, S. Sandoval, F. Quisaguano, and A. Limaico, "Visual SLAM with a RGB-D camera on a quadrotor UAV using on-board processing," in *Proc. Int. Work-Conf. Artif. Neural Netw.*, 2017, pp. 596–606.

[11] Z. Wang, S. Liu, G. Chen, and W. Dong, "Robust visual positioning of the UAV for the under bridge inspection with a ground guided vehicle," in *IEEE Trans. Instrum. Meas.*, vol. 71, pp. 1–10, 2022.

[12] Ho, M. Hui, S. H. Liao, and C. C. Chiu, "UWB communication characteristics for different distribution of people and various materials of walls," *J. Appl. Sci. Eng.*, vol. 13, no. 3, pp. 315–326, Sep. 2010.

[13] N. Zhou, M. Si, D. Li, C. Seow, and J. Mi, "An indoor UWB 3D positioning method for coplanar base stations," *Sensors*, vol. 22, no. 24, p. 9634, 2022.

[14] R. M. Rao, A. V. Padaki, B. L. Ng, Y. Yang, M.-S. Kang, and V. Marojevic, "ToA-based localization of far-away targets: Equi-DOP surfaces, asymptotic bounds, and dimension adaptation," *IEEE Trans. Veh. Technol.*, vol. 70, no. 10, pp. 11089–11094, Oct. 2021.

[15] Y. Guo, W. Li, G. Yang, Z. Jiao, and J. Yan, "Combining dilution of precision and Kalman filtering for UWB positioning in a narrow space," *Remote Sens.*, vol. 14, no. 21, p. 5409, 2022, doi: 10.3390/rs14215409.

[16] J.-H. Bai, J.-Y. Han, and R.-B. Wu, "A GPS-free bridge inspection method tailored to bridge terrain with high positioning stability," *IEEE Trans. Aerospace Electron. Syst.*, to be published.

[17] Y. T. Chan and K. C. Ho, "A simple and efficient estimator for hyperbolic location," *IEEE Trans. Signal Process.*, vol. 42, no. 8, pp. 1905–1915, Aug. 1994.

[18] W. H. Foy, "Position-location solutions by Taylor-series estimation," *IEEE Trans. Aerosp. Electron. Syst.*, no. 2, pp. 187–194, Mar. 1976.

[19] Y.-E. Chen, H.-H. Liew, J.-C. Chao, and R.-B. Wu, "Decimeter-accuracy positioning for drones using two-stage trilateration in a GPS-denied environment," *IEEE Internet Things J.*, vol. 10, no. 9, pp. 8319–8326, May 2023.

[20] H. Hu, X. Yang, R. Liu, L. Liu, and H. Hu, "Study on the deployment of ultra-wideband positioning base stations in pig farms," *Appl. Sci.*, vol. 14, no. 2, no. 501, Jan. 2024.

[21] Z. Karimi. "Confusion matrix." Accessed: Oct. 4, 2024. [online] Available: http://www.researchgate.net/publication/355096788

Chia-Lun Tsai was born in Taipei, Taiwan. He received the B.S degree in communication engineering from National Central University, Taoyuan City, Taiwan, in 2021, and the M.S degree in communication engineering from National Taiwan University, Taipei, Taiwan, in 2024.

His research interests are inclined to be related to the field of UAV localization and outlier detection.

Ruey-Beei Wu (Life Fellow, IEEE) was born in Tainan, Taiwan. He received the B.S. and Ph.D. degrees from the Department of Electrical Engineering, National Taiwan University, Taipei, Taiwan, in 1979 and 1985, respectively.

He joined the Faculty with the Department of Electrical Engineering, National Taiwan University in 1982. He has also been with the Graduate Institute of Communications Engineering since its establishment in 1997. He was a Postdoctoral Researcher with IBM, East Fishkill, NY, USA, in 1986, was a Visiting Professor with the University of California at Los Angeles, Los Angeles, CA, USA, in 1994, and also with Gent University, Ghent, Belgium, in 2009. He was appointed as the Director of the National Center for High performance Computing from 1998 to 2000 and the Director General of the Planning and Evaluation Department from 2002 to 2004, both under the National Science Council. He also served as the President of the Institute for Information Industry from 2012 to 2016. His areas of interest include computational electro-magnetics, transmission line and waveguide discontinuities, and microwave and millimeter wave passive components and electromagnetic design for advanced packaging and systems.

Dr. Wu received the NSC Distinguished Research Awards in 1990, 1993, 1995, and 1997, respectively, and was given the Outstanding Electrical Engineering Professor Award by the Chinese Institute of Electrical Engineers in 1999. He received the Best Paper Award from IEEE Transactions on Advanced Packaging in 2009, the Outstanding Research Award from the Pan Wen Yuan Foundation in 2013, and the Academic Award from the Ministry of Education in 2013. He served as an Associate Editor for the IEEE TRANSACTIONS ON MICROWAVE THEORY AND TECHNIQUE from 2005 to 2008 and the IEEE TRANSACTIONS ON ADVANCED PACKAGING from 2009 to 2012. He served as the Chair for the IEEE Taipei Section from 2007 to 2009 and received the MGA Outstanding Large Section Award and the Innovation Award in 2009.